First-Principles Study on Electronic Structure and Magnetic Interactions in Ni-doped CdS

Yanrui Guo*, Huiyu Yan, Qinggong Song, Wei Kong and Fang Yang

College of Science, Civil Aviation University of China, Tianjin 300300, China

Received: 09.11.2020 & Accepted: 28.05.2021

Doi: 10.12693/APhysPolA.140.3 *e-mail: yanrui_g@163.com

By using the first-principles calculation method, the electronic structure and magnetic interactions of Ni-doped wurtzite CdS have been investigated. The results reveal that the ground state of the system is a spin polarized state. The magnetic moment of Ni-doped CdS is 2.0 μ_B per cell, which mainly comes from Ni and its neighbor S atoms. Various configurations of Ni-doped CdS show half-metallic characters with a 100% spin polarization. Ni-doped wurtzite CdS presents a long-range ferromagnetic coupling. These results indicate that Ni-doped wurtzite CdS is a promising spin electronic material.

topics: first principles, Ni-doped wurtzite CdS, electronic structure, ferromagnetic coupling

1. Introduction

During the past decades, dilute magnetic semiconductors (DMSs) have attracted much attention due to their potential as a new functional material, paving the way for the introduction of spin into semiconductor devices [1, 2]. Generally, the primary purpose is searching for DMSs with intrinsic ferromagnetism and the Curie temperature (T_C) higher than room temperature (RT). For this purpose, DMSs with RT ferromagnetic (FM) property, which consisted of a semiconductor doped by $3d$ transition metal (TM) or nonmagnetic elements, have been realized experimentally, such as Cr-doped ZnTe and GaN [3, 4], TMs-doped ZnO, TiO_2, SnO_2, Ti_2NiAl [5–10]. However, the origin of RT ferromagnetism can be from intrinsic magnetic behaviors, precipitation of magnetic clusters or the secondary magnetic phases, which is still under debate [11]. These extrinsic magnetic behaviors are undesirable for practices. In order to understand the origin of ferromagnetism in DMSs, many research groups have studied the influence of doping and vacancy on FM properties by using the first-principles calculation method [10–13].

Cadmium sulfide (CdS) is a famous II–VI semiconductor material due to its excellent photoelectric properties. CdS films have been widely used in sensors, solar cells, nonlinear integrated optical devices and other fields [14, 15]. As already reported, CdS-based DMSs can be realized by transition metals Mn, Fe, Co and some nonmagnetic dopants as well [16–19]. However, these studies mainly focus on CdS with a zinc blende structure, while there is a shortage of research related to wurtzite CdS.

Therefore, in this paper, based on the first-principles calculation method, the electronic structure and magnetic properties of Ni-doped wurtzite CdS are analyzed, and the origin of its magnetism is also discussed. The calculated results show that Ni-doped wurtzite CdS presents a 100% spin polarization. This research not only helps us to understand the origin of ferromagnetism of DMSs but also supplements the diluted magnetic semiconductor materials.

2. Details of calculations

Geometry optimization and energy calculations were performed using density functional theory (DFT) with a plane wave expansion in the Cambridge Serial Total Energy Package (CASTEP) code [20]. The interaction between the electrons and the ionic core is described by an ultrasoft pseudo-potential [21]. The electron–electron exchange and correlation effects are described by the Perdew–Burke–Ernzerhof (PBE) scheme in the generalized gradient approximation (GGA) with and without Hubbard U [22, 23]. The valence electrons for S, Cd, and Ni are chosen as $3s^2 3p^4$, $4d^{10}5s^2$ and $3d^8 4s^2$, respectively. The energy cutoff is set to 300 eV, and a Monkhorst–Pack grid with parameters of $3 \times 3 \times 3$ was used for the irreducible

TABLE I

The calculated lattice parameters, total energies of intrinsic and Ni-doped CdS.

	a [Å]	c [Å]	β	$E_{\rm tot}$ [eV]	$E_{\rm g}$ [eV]
CdS in Ref. [24, 25]	4.135	6.749			2.42
intrinsic CdS	4.227	6.878	120.000	−3126.08447	1.13
Ni–CdS (non-spin polarized state)	4.198	6.840	120.004	−56340.53833	
Ni–CdS (spin polarized state)	4.202	6.834	120.004	−56340.82591	

Brillouin zone. In the geometry optimization process, the SCF tolerance, the maximum tolerances of the force, stress, and displacement were set to 0.5×10^{-6} eV/atom, 0.01 eV/Å, 0.02 GPa and 0.5×10^{-3} Å, respectively.

It should be noted that both LDA and GGA schemes tend to underestimate the bandgap and give a strong FM coupling interaction [22, 23]. This is caused by the overestimation of delocalization of wave function. There are many approaches to relieve the dilemma, including hybrid potentials methods and the DFT+U scheme [23]. In this paper, besides GGA calculations, GGA+U calculations are also performed to study the magnetic interactions.

In GGA+U calculations, when considering the localization of Ni 3d, Cd 4d and S 2p electrons, and in order to cater for the bandgap of CdS in experiments [24, 25], the on-site Coulomb repulsion $U = 7.2$ eV and $U = 3.87$ eV is applied to Cd 4d and S 2p state, respectively. For the Ni 3d state, there is no experimental value in Ni-doped wurtzite CdS and there is also no theoretical research. Here, in our GGA+U calculations, we used the same value $U = 7.2$ eV to the Ni 3d state and Cd 4d state, as it was done in other studies [26, 27].

CdS can present a hexagonal wurtzite structure (space group $P63mc$) with lattice constants $a = 4.14$ Å, $c = 6.71$ Å, as reported by [24]. Based on a conventional wurtzite CdS cell, we build a $3 \times 3 \times 2$ CdS supercell (72 atoms) as a matrix for the doped system, which contains 36 Cd atoms and 36 S atoms, as shown in Fig. 1.

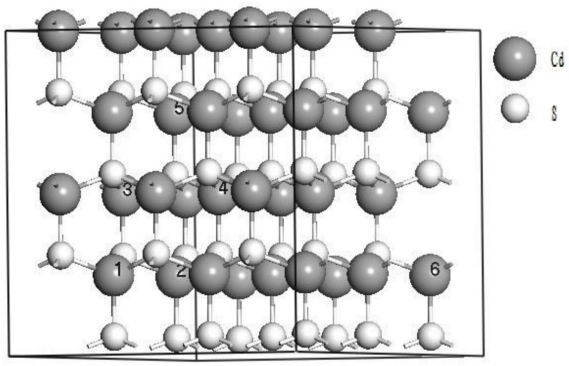

Fig. 1. The supercell structure of CdS.

3. Results and discussion

3.1. Geometry optimization

Firstly, the geometry optimization of CdS is performed, and the results show that the lattice constants a and c are 4.227 Å and 6.878 Å, respectively. These results are in good agreement with the experimental values ($a = 4.135$ Å, $c = 6.749$ Å) [24, 25] which means that our calculation model and calculation settings are reasonable. The Ni-doped CdS model is established in such a way that a Ni atom replaces a Cd atom in a 72 atom supercell. With geometry optimizations, we can get the energies of doped systems with a spin polarized state and a non-spin polarized state, respectively, as shown in Table I. One can see there that the total energy of the $Cd_{35}NiS_{36}$ system with the spin polarized state is lower than that with the non-spin polarized state. Therefore, the ground state of Ni-doped CdS is spin polarized. It can also be seen from Table I that the lattice parameters slightly decrease after Ni doping, which can be related to the fact that the ion radius of Ni is 0.73 Å smaller than that of Cd (0.95 Å). Moreover, the calculated bond length of Ni–S in the NiS_4 tetrahedron is 2.32 Å, i.e., 0.27 Å smaller than for Cd–S (2.59 Å) in the CdS_4 tetrahedron. This can also contribute to the difference of lattice parameters.

To test whether CdS can be doped by Ni atoms, the formation energy of the doped system is calculated using [28, 29]

$$E_{\rm form} = E_{\rm Ni-CdS} - E_{\rm CdS} - \mu_{\rm Ni} + \mu_{\rm Cd}. \quad (1)$$

Here, $E_{\rm Ni-CdS}$ is the total energy of the doped system, $E_{\rm CdS}$ is the total energy of intrinsic CdS, $\mu_{\rm Ni}$ and $\mu_{\rm Cd}$ are the chemical potentials of Ni and Cd atom, respectively. The μ_{Ni} is equal to the energy of one Ni atom in Ni bulk. Under cadmium-rich conditions, the chemical potential of cadmium is approximately equal to the energy of a Cd atom in the bulk of metal Cd. Under sulfur-rich conditions, the chemical potential of S is equal to the energy of an S atom in S bulk. Hence, the chemical potential of Cd can be obtained by the relation

$$\mu_{\rm Cd} = E_{\rm CdS} - \mu_{\rm S}, \quad (2)$$

where $\mu_{\rm S}$ is the chemical potential of S. The formation energy of Ni-doped CdS has been calculated under high cadmium and sulfur conditions, respectively. The results show that the formation energy

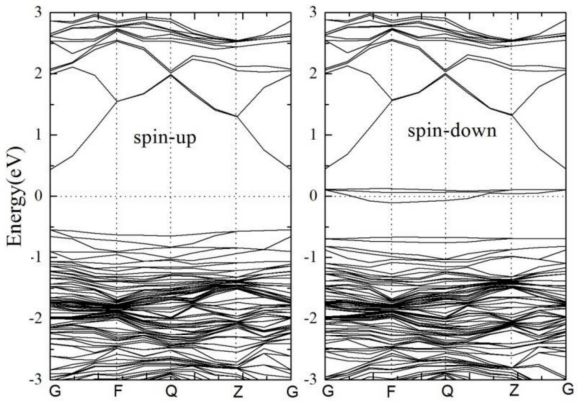

Fig. 2. Band structures of the spin-up and the spin-down of $Cd_{35}NiS_{36}$. The zero energy corresponds to the Fermi energy.

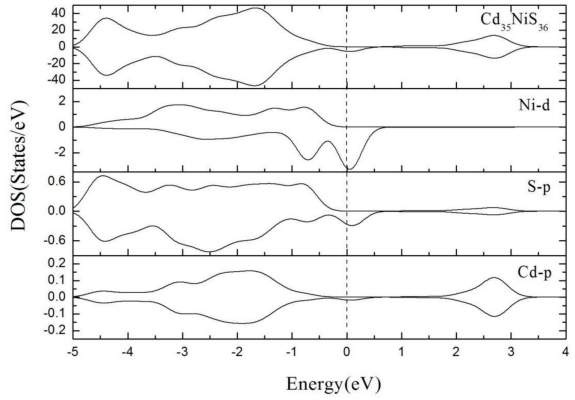

Fig. 3. Total DOS of $Cd_{35}NiS_{36}$, partial DOSs of Ni d, S p and Cd p. The zero energy corresponds to the Fermi energy.

of Ni-doped CdS is (i) 1.95 eV under cadmium-rich conditions, (ii) 0.60 eV under sulfur-rich conditions, which turn out to be far less than the formation energy of the C-doped CdS system (1.2 eV) [16], and also less than the formation energy of the Cu-doped CdS system (0.73 eV) [29]. One can conclude that in the case of rich sulfur, the structure where Ni replaces Cd is more stable and can be easily fabricated in experiments.

3.2. Electronic properties of Ni-doped CdS

The band structure of Ni-doped CdS is shown in Fig. 2, from which it can be seen that the Ni dopant can introduce a new impurity energy level into the spin-down band gap. Note that the impurity energy level only appears in the spin-down band, indicating that the doping system presents the half-metallic characteristics with a 100% spin polarization.

In order to clarify the contribution of different atoms in the Ni-doped CdS system to the spin state, the total and partial density of states (DOSs) of $Cd_{35}NiS_{36}$ are analyzed (see Fig. 3). There are obvious overlaps among the Ni d, S p and Cd p states

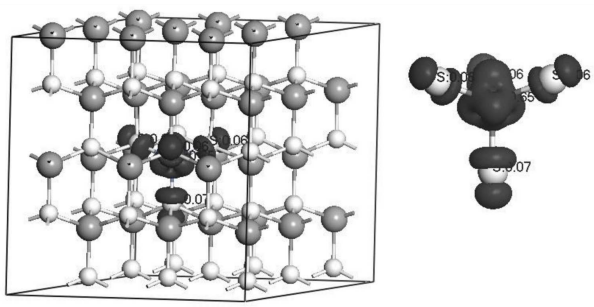

Fig. 4. Spin density distribution of Ni and its surrounding.

near the Fermi level, indicating that there is a strong p–d hybridization between them. These strong interactions can respond to the splitting of energy levels near the Fermi level. Ni-doped CdS has a total magnetic moment of 2.0 μ_B, in which most of the magnetic moments are localized in the NiS_4 tetrahedron. The spin density distribution is shown in Fig. 4. We found that the magnetic moment localized on Ni atom is 0.65 μ_B, and the remaining part comes mainly from the nearest sulfur atom around the Ni dopant. The magnetic moment provided by S at the vertex of the NiS_4 tetrahedron is 0.07 μ_B, where the magnetic moment contributed by each S atom is 0.06 μ_B.

3.3. Magnetic coupling of two Ni-doped CdS systems

To test the ferromagnetic properties of Ni-doped CdS, the magnetic coupling characteristics of Ni doped system have been studied. We replaced two Cd by two Ni atoms, considering different configurations in the $3 \times 3 \times 2$ CdS supercell. These configurations are $(1,2)$, $(1,3)$, $(1,4)$, $(1,5)$, and $(1,6)$, where the numbers 1–6 indicate the positions of the replaced Cd atoms (see Fig. 1). With full geometry optimization of each configuration, the distance between Ni–Ni pairs in the five configurations is 4.10, 3.99, 5.99, 7.98, and 7.32 Å, respectively. The energy calculations of the FM and antiferromagnetic (AFM) states of various configurations were performed and the results are shown in Table II, where d_{Ni-Ni} represents the distance between Ni and Ni, and M is the total magnetic moment of the double doping system. We use $\Delta E = E_{AFM} - E_{FM}$ as the criterion of ferromagnetic stability. If ΔE is positive, the ferromagnetic state of the structure is more stable; otherwise, the antiferromagnetic state is the prior state.

Our results show that ΔE is greater than zero for all configurations, therefore proving that the ground state of Ni-doped wurtzite CdS prefers a ferromagnetic state. The magnetic moment of various configurations is kept at 4.0 μ_B. This means that the half-metal property of Ni-doped CdS presents robustness — a feature important for the application of spin electronics. We may also note in Table II

TABLE II

Summary of total energies of FM and AFM states, magnetic moments and energy differences ($\Delta E = E_{\mathrm{AFM}} - E_{\mathrm{FM}}$) for different configurations of $Cd_{34}Ni_2S_{36}$ with GGA and GGA+U.

Configuration	$d_{\mathrm{Ni-Ni}}$ [Å]	GGA				GGA+U
		M [μ_{B}]	E_{FM} [meV]	E_{AFM} [meV]	ΔE [meV]	ΔE [meV]
$(1,2)$	4.10198	4.00	22.05	140.94	118.89	−5.77
$(1,3)$	3.99422	4.00	0	539.51	539.51	1.11
$(1,4)$	5.98655	4.00	183.43	223.64	40.22	−24.82
$(1,5)$	7.98203	4.00	211.68	1240.49	1028.81	53.36
$(1,6)$	7.32191	4.00	197.26	812.45	615.19	12.89

that the ferromagnetic state of the $(1,3)$ configuration has the lowest energy as compared to other configurations so that the total energies are interpreted relative to that of the configuration $(1,3)$ with the FM state. Meanwhile, since the distance between Ni and Ni in the $(1,3)$ configuration is the shortest, the two Ni atoms tend to occupy the nearest neighbor position, causing the cluster-like effect.

It is interesting that the $(1,5)$ configuration, in which the distance between Ni and Ni is the longest (7.98 Å), takes the strongest FM coupling with $\Delta E = 1028.81$ meV. A long-range interaction of FM is therefore justified. Due to the periodic properties of models, the magnetic coupling would be then modulated by the neighbor supercell. The $(1,5)$ configuration would be affected by the neighbor unit the most because of the largest distance between Ni dopants as compared to other calculated configurations. Nevertheless, the FM coupling can still be regarded as a long-range interaction since the distance between the Ni dopant at site 1 in the neighbor unit and the Ni dopant at site 5 nearly equals the Ni–Ni distance in the $(1,5)$ configuration.

To study the source of ferromagnetism and long-range ferromagnetism of Ni-doped CdS, we mapped the spin resolved band structure of configuration $(1,3)$. This is shown in Fig. 5, from which we can find all the defect levels presenting the main spin states. The 100% spin polarization rate can be responsible for the integer magnetic moment of the system. The spin density distribution of configuration $(1,3)$ of $Cd_{34}Ni_2S_{36}$ is shown in Fig. 6. There, one can see that spin coupling between the Ni–Ni pair can be realized by a bridge connecting the S atom due to the strong p–d coupling. As a result, Ni atoms take the same spin orientation, inducing a strong ferromagnetic coupling between them.

To further elucidate the origin of ferromagnetism of Ni-doped CdS, in Fig. 7 we have presented the spin density distribution of configuration $(1,5)$ which shows the maximum Ni–Ni distance among all configurations. The ferromagnetic coupling between Ni atoms at such a large distance cannot be explained by double exchange or super exchange interaction. Our suggestion is that the Cd atom between two NiS_4 tetrahedrons modulates the ferromagnetic coupling between Ni and Ni. Note that

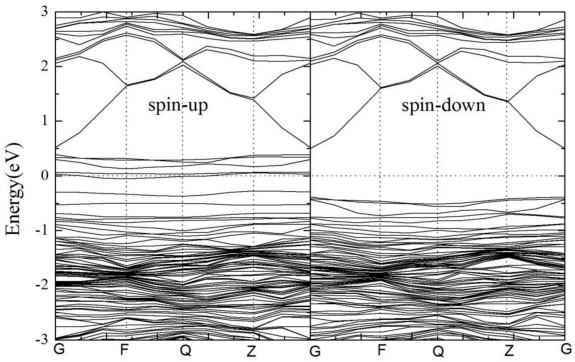

Fig. 5. Band structures of Ni and its surrounding for configuration $(1,3)$ $Cd_{34}Ni_2S_{36}$. The zero energy corresponds to the Fermi energy.

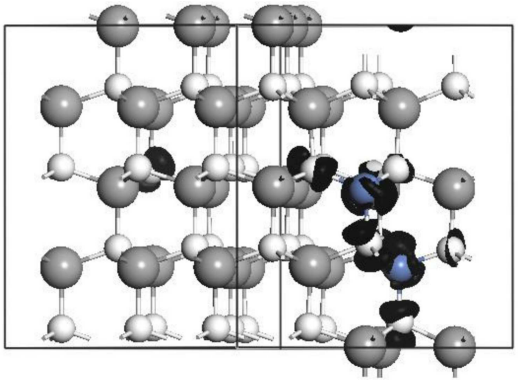

Fig. 6. Spin density distribution of Ni and its surrounding for configuration $(1,3)$ $Cd_{34}Ni_2S_{36}$.

a strong p–d hybrid between Ni and the nearest S atom affects the spin polarization of the S atom, and such hybridization can modulate the ferromagnetic coupling between Ni atoms. The second nearest neighbor Cd atom is coupled with the third nearest S atom, and the third nearest S atom is similarly coupled with its nearest Ni atom, so it gives the Ni $3d$–S $3p$–Cd–S $3p$–Ni $3d$ interaction chain. This chain of action can be responsible for the long-range coupling between Ni and Ni.

The modified ΔE values of various configurations computed using GGA+U are listed in Table II. We found that the Coulomb interaction has a strong

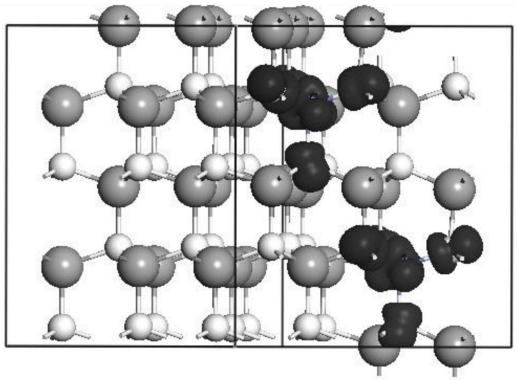

Fig. 7. Spin density distribution of Ni and its surrounding for configuration $(1,5)$ $Cd_{34}Ni_2S_{36}$.

influence on ferromagnetic coupling in Ni-doped CdS. The magnetic Ni–Ni interaction obtained with the GGA+U method is much smaller than that obtained with the GGA method. This may originate from the enhancement of localization of corresponding wave functions. As a result, the spatially extended states of electrons decrease, inducing a smaller exchange interaction between Ni impurities. Similar observations were made in [26]. However, in some other reports, the Hubbard U can enhance magnetic coupling interactions [30]. As the influence of Hubbard U on ferromagnetic stability is absorbing, more detailed research is needed.

The tendency of the coupling strength to vary depending on configurations, shown by the GGA+U method, is similar to that of the GGA method.

For example, configuration $(1,2)$ and $(1,3)$ present the AFM and the FM ground state, respectively, both, however, take the form of the Ni–S–Ni bridge. This may come from the anisotropy of wurtzite CdS. Configuration $(1,5)$ remains in the FM ground state under the GGA+U calculations, also indicating the long-range interaction of the FM coupling in Ni-doped CdS.

It should be noted that in many DMSs, the spin polarization of 100% can be realized only in the case of a supercell with one dopant atom. In the case of the supercell with dopant pair configurations, the spin polarization of 100% is destroyed. In fact, this greatly hinders the application prospect of DMSs. However, in the case of Ni-doped CdS in this work, we have found that all configurations of the supercell with Ni pairs present a 100% spin polarization. Moreover, as mentioned above, Ni-doped CdS presents a long-range ferromagnetic coupling. These results show that Ni-doped CdS is a promising spin electronic material.

4. Conclusions

Based on the first-principles method of density functional theory, the electronic structure and magnetic properties of Ni-doped wurtzite CdS were studied. The results showed that the ground state of the considered system is a half-metal with a 100% spin polarization. A nitrogen dopant can introduce a magnetic moment of 2.0 μ_B, which comes mainly from the NiS_4 tetrahedron. All configurations of Ni-doped wurtzite CdS allow for keeping a 100% spin polarization. Also, the long-range ferromagnetic coupling could be realized in Ni-doped wurtzite CdS.

Acknowledgments

This work was financially supported by the National Natural Science Foundation of China (grant No. 11805272) and the Foundation of the Civil Aviation University of China (grant No. 3122017081).

References

[1] H. Raebiger, H. Nakayama, T. Fujita, *J. Appl. Phys.* **115**, 012008 (2014).

[2] X.J. Yang, Y.K. Li, C.Y. Shen, B.Q. Si, Y.L. Sun, Q. Tao, G.H. Cao, Z. Xu, F.C. Zhang, *Appl. Phys. Lett.* **103**, 022410 (2013).

[3] H. Saito, V. Zayets, S. Yamagata, K. Ando, *Phys. Rev. Lett.* **90**, 207202 (2003).

[4] R.K. Singh, S.Y. Wu, H.X. Liu, L. Gu, D.J. Smith, N. Newman, *Appl. Phys. Lett.* **86**, 012504 (2005).

[5] L.M.C. Pereira, J.P. Araújo, U. Wahl, S. Decoster, M.J. Van Bael, K. Temst, A. Vantomme, *J. Appl. Phys.* **113**, 023903(2013).

[6] X.P. Wei, Y.D. Chu, X.W. Sun, Y.E.T. Song, P. Guo, *Acta Phys. Pol. A* **126**, 795 (2014).

[7] J.D. Bryan, S.M. Heald, S.A. Chambers, D.R. Gamelin, *J. Am. Chem. Soc.* **126**, 11640 (2004).

[8] K.C. Zhang, Y.F. Li, Y. Liu, F. Chi, *J. Appl. Phys.* **114**, 133707 (2013).

[9] H.X. Luan, C.W. Zhang, F. Li, P. Li, M.J. Ren, M. Yuan, W.X. Ji, P.J. Wang, *RSC Adv.* **4**, 9602 (2014).

[10] M.E. Victor, L.P. William, G.H. Rafael, G.G. Alvaro, *Physica B* **557**, 74 (2019).

[11] T. Dietl, *J. Appl. Phys.* **103**, 07D111 (2008).

[12] Y.F. Chen, W.B. Mi, J.F. Yang, Q.G. Song, H.Y. Yan, T. Wei, Y.R. Guo, *Solid State Commun.* **205**, 9 (2015).

[13] Q.G. Feng, *J. Phys.* **32**, 445602 (2020).

[14] T. Mandal, C. Dasgupta, P.K. Mait, *Phys. Rev. B* **91**, 104107 (2015).

[15] L. Biadala, H. Frederich, L. Coolen, S. Buil, X. Quélin, C. Javaux, M. Nasilowski, B. Dubertret, J.-P. Hermier, *Phys. Rev. B* **91**, 085416 (2015).

[16] H. Pan, Y.P. Feng, Q.Y. Wu, Z.G. Huang, J.Y. Lin, *Phys. Rev. B* **77**, 125211 (2008).

[17] H.V. Anh, N.H. Cuong, N. Tu, L.M. Tuan, D.X. Nui, N.D. Dung, N.D.T. Kien, P.T. Huy, D.X. Viet, *J. Alloys Compd.* **695**, 1624 (2017).

[18] C.T. Tsai, S.H. Chen, D.S. Chuu, W.C. Chou, *Phys. Rev. B* **54**, 11555 (1996).

[19] V. Ladizhansky, V. Lyahovitskaya, S. Vega, *Phys. Rev. B* **60**, 8097 (1999).

[20] M.D. Segall, P.J.D. Lindan, M.J. Probert, C.J. Pickard, P.J. Hasnip, S.J. Clark, M.C. Payne, *J. Phys.* **14**, 2717 (2002).

[21] D. Vanderbilt, *Phys. Rev. B* **41**, 7892 (1990).

[22] J.P. Perdew, K. Burke, M. Ernzerhof, *Phys. Rev. Lett.* **77**, 3865 (1996).

[23] V.I. Anisimov, F. Aryasetiawan, A.I. Lichtenstein, *J. Phys. Condens. Matter* **9**, 767 (1997).

[24] A. Nabi, W. Akram, A. Majid, G. Nabi, *J. Comput. Intell. Electron. Syst.* **2**, 116 (2013).

[25] A.I. Oliva, O. Solis-Canto, R. Castro-Rodriguez, P. Quintana, *Thin Solid Films* **391**, 28 (2001).

[26] W.-Zh. Xiao, L.-L. Wang, L. Xu, Q. Wan, A.L. Pan, H.Q. Deng, *Physica B* **405**, 4858 (2010).

[27] I.S. Elfimov, A. Rusydi, S.I. Csiszar, Z. Hu, H.H. Hsieh, H.-J. Lin, C.T. Chen, R. Liang, G.A. Sawatzky, *Phys. Rev. Lett.* **98**, 137202 (2007).

[28] Q.J. Wang, J.B. Wang, X.L. Zhong, Q.H. Tan, Z. Hu, Y.C. Zhou, *Appl. Phys. Lett.* **100**, 132407 (2012).

[29] P. Li, C.W. Zhang, J. Lian, S. Gao, X. Wang, *Solid State Commun.* **151**, 1712 (2011).

[30] L. Lin, R. Chen, C.Z. He, H.L. Tao, J.T. Huang, L.H. Zhu, L.B. Yan, J.S. Zhang, *Vacuum* **182**, 109681 (2020).